Unsupervised Detection of Pulmonary Opacities for Computer-Aided Diagnosis of COVID-19 on CT Images

Rui Xu[*†‡], Xiao Cao[§†], Yufeng Wang[§†], Yen-Wei Chen[¶†], Xinchen Ye[*†‡], Lin Lin[*†‡],
Wenchao Zhu[‖], Chao Chen[‖], Fangyi Xu[‖], Yong Zhou[‖], Hongjie Hu[‖], Shoji Kido[**] and Noriyuki Tomiyama[**]

[*]DUT-RU International School of Information Science & Engineering, Dalian University of Technology, Dalian, China
[†]DUT-RU Co-Research Center of Advanced ICT for Active Life, Dalian, China
[‡]Key Laboratory for Ubiquitous Network and Service Software of Liaoning Province, Dalian, China
[§]College of Software, Dalian University of Technology, Dalian, China
[¶]College of Information Science and Engineering, Ritsumeikan University, Kusatsu, Japan
[‖]Department of Radiology, Sir Run Run Shaw Hospital, Zhejiang University School of Medicine, Hangzhou, China
[**]Department of Diagnostic and Interventional Radiology, Graduate School of Medicine, Osaka University, Osaka, Japan

Abstract—**COVID-19 emerged towards the end of 2019 which was identified as a global pandemic by the world heath organization (WHO). With the rapid spread of COVID-19, the number of infected and suspected patients has increased dramatically. Chest computed tomography (CT) has been recognized as an efficient tool for the diagnosis of COVID-19. However, the huge CT data make it difficult for radiologist to fully exploit them on the diagnosis. In this paper, we propose a computer-aided diagnosis system that can automatically analyze CT images to distinguish the COVID-19 against to community-acquired pneumonia (CAP). The proposed system is based on an unsupervised pulmonary opacity detection method that locates opacity regions by a detector unsupervisedly trained from CT images with normal lung tissues. Radiomics based features are extracted insides the opacity regions, and fed into classifiers for classification. We evaluate the proposed CAD system by using 200 CT images collected from different patients in several hospitals. The accuracy, precision, recall, f1-score and AUC achieved are 95.5%, 100%, 91%, 95.1% and 95.9% respectively, exhibiting the promising capacity on the differential diagnosis of COVID-19 from CT images.**

Index Terms—**COVID-19, CT images, Unsupervised detection of pulmonary opacities, Computer-aided diagnosis**

I. INTRODUCTION

Since December 2019, the outbreak of severe acute respiratory syndrome coronavirus (SARS-COV-2) [1] has caused millions of cases of Corona Virus Disease (COVID-19) in the world. The world health organization (WHO) has announced that the COVID-19 as a global healthy emergency on January 30, 2020. [2]. As a form of pneumonia, COVID-19 causes fever, cough or respiratory symptoms, making the patient difficult to breathe. Other symptoms are vomiting, diarrhea, myalgia pleurisy, etc. Currently, the diagnosis of COVID-19 is mainly based on the test of real-time poly-merase chain reaction (RT-PCR). However, recent studies show that RT-PCR has a low positive and sensitivity rate in the early stage of COVID-19 [3] [4] which may miss the early diagnosis of COVID-19. On the other hand, using RT-PCR to confirm COVID-19 patients is time-consuming and is limited by the lack of supply test kits. The computed tomography (CT) imaging, as a routine diagnostic tool for pneumonia, plays a critical role in the diagnosis of COVID-19 [5]. Compared with the RT-PCR, it is easier and faster to take a chest CT scanning, which makes the diagnosis of COVID-19 more available and economic. However, a chest CT image usually contains several hundred of CT slices in lung regions, which takes radiologists a lot of time to review all slices. Besides, the fast growth of COVID-19 patients further make it hard to carefully check huge amounts of CT images, which could cause mis-diagnosis. Therefore, it is required to develop a computer-aided diagnosis system that can automatically analyze CT images to help radiologists for the COVID-19 diagnosis.

There have been some works related to the CAD system of COVID-19 on CT images. For example, the works [6] [7] [8] [9] [10] utilize deep learning based techniques to automatically analyze CT images for differential diagnosis of COVID-19 against to community-acquired pneumonia (CAP). These methods have demonstrated the potential ability of deep learning in the diagnosis of COVID-19, but they extract features from the entire CT images rather than focusing on the regions of pulmonary opacities caused by pneumonia, which limits their performances. Other works present opacity-aware methods [11] [12] [13], which make the feature extraction to be restricted inside the regions of pulmonary opacities. The experimental results demonstrate that the capacity of COVID-19 diagnosis can be improved by leveraging the location-specific features. The opacity regions can be obtained by supervisedly training a deep network for opacity region segmentation [13], which requires the human annotation of these regions on a lot of CT images. This not only costs too much time and human labors, but also make it hard for researches in academics to develop self-motivated tools for their study of COVID-19.

In this study, we propose an unsupervised learning method that can easily train a detector to locate regions of pulmonary opacities on CT images. We exploit an anomaly detection

based framework [14] to train the opacity detector by using several tens of CT images with normal lung tissues. Since the detector only sees normal CT images during the training, it is able to detect abnormality (pulmonary opacities) when a CT image exhibits radiological features of COVID-19 or CAP. Besides, we apply the unsupervised detection of pulmonary opacity to develop a CAD system for differential diagnosis of COVID-19. Radiomics-based features are extracted inside the detected opacity regions on CT images and LASSO-based feature selection [15] is carried out to choose a few number of optimal features. Several widely-used classifiers are trained and compared to distinguish COVID-19 and CAP. We evaluate the developed CAD system by using 200 CT images collected from different patients in several hospitals. The main contributions of this paper are as follows:

- We present an unsupervised learning method to detect pulmonary opacities on CT images, which saves huge labors of manual annotation of opacity regions.
- We apply the unsupervised detection of pulmonary opacity to develop a CAD system to distinguish COVID-19 and CAP on CT images.

II. RELATED WORK

A. Deep learning based diagnosis of COVID-19

Since the outbreak of COVID-19, there are several deep learning based methods that have been proposed for diagnosis of COVID-19 and achieved very promising classification accuracy. Zheng et al. [6] established a 3D CNN (DeCoVNet) to predict the probability of COVID-19 infectious. Wang et al. [7] modified the Inception network and make use of transfer learning to distinguish COVID-19 and typical pneumonia in chest CT scans. Ozkaya et al. [8] use pre-trained CNN models to extract features from CT scans and propose a feature fusion and ranking method to improve the performance. Kassani et al. [9] choose a pool of CNN models to extract features from X-ray and CT images and feed them into several machine learning classifiers to classify COVID-19 cases. Farooq et al. [10] propose a pre-trained ResNet-50 architecture, called COVID-ResNet for differentiating COVID-19 cases from other pneumonia cases. Different data augmentation methods are used to improve the generalization of the training model. Sun et al. [11] propose a feature selection method and is incorporated with a deep forest model for COVID-19 vs. CAP classification by using the chest CT images. Experimental results show that the proposed approach can achieve superior performance compared with other widely used machine learning methods. Ouyang et al. [12] develop a 3D CNN model combined with a novel attention module to automatically diagnose COVID-19 from CAP. By focusing on the infection regions in lungs, the proposed algorithm achieves generalization performance on multi-center CT data. Shi et al. [13] leverage VB-Net to obtain the segmentation results of infection and lung regions which are used for feature extraction. A series of handcrafted features are designed for random forest to screen COVID-19 from CAP.

B. Anomaly detection

Anomaly detection aims at identifying abnormal cases by training only on normal data which is widely used in computer vision [14] and medical field. With the development of deep learning, recent works mainly based on auto-encoders (AEs) and generative adversarial network (GAN). The main idea is to use these generative models to learn the distribution of normal data and identify anomalies as samples with high reconstruction errors. Based on related ideas, there are a number of works proposed in medical field. Pawlowski et al. [16] explore the use of Bayesian AEs to detect lesions in brain CT scans. Schlegl et al. [17] propose AnoGAN to map an image with abnormality to the latent space and then reconstruct this representation back to image. The difference between reconstructed and the test image is used to compute abnormality score. Chen et al. [18] add a constraint in latent space representation to adversarial AEs to encourage latent space consistency for unsupervised detection of tumor in brain MRI. Chen et al. [19] include KL-term for reducing the difference between reconstructed and original image on normal data. Baur et al. [20] and Sato et al. [21] make use of AEs based models for detecting abnormal regions through reconstruction error.

III. METHOD

Fig. 1 illustrates the whole procedure of our developed CAD system for the diagnosis of COVID-19 on CT images. It can be roughly divided into the following steps, which are lung segmentation, opacity detection, feature extraction and classification. At first, lung regions are extracted from CT images by using a deep convolutional network that is trained on a mixed dataset comprised by public and private CT images. Then, we exploit an anomaly detection based framework to extract the opacity regions via an unsupervised learning manner. The opacity detector is based on a auto-encoder that is trained by only using CT images with normal tissues. Since the auto-encoder is only familiar with normal CT images, it can not reconstruct well for abnormal CT images with pulmonary opacities. By exploiting the reconstruction errors and the segmented lung regions, it is easy to detect the opacity regions, where feature extraction is conducted. Finally, feature vectors are fed into a classifier to distinguish COVID-19 and CAP. We describe the details of each part in this section.

A. Lung Segmentation

We present a high-accuracy network for the segmentation of COVID-19 lung regions from chest CT images. A mixed dataset is constructed for improving the generalizability of the segmentation network.

Models. Ronneberger et al. [22] proposed the U-Net for segmentation of microscopy images. In this study, we utilize the U-Net architecture with different pre-trained encoders as backbone, such as MobileNetV2 [23], VGG19 [24] and ResNet50 [25].
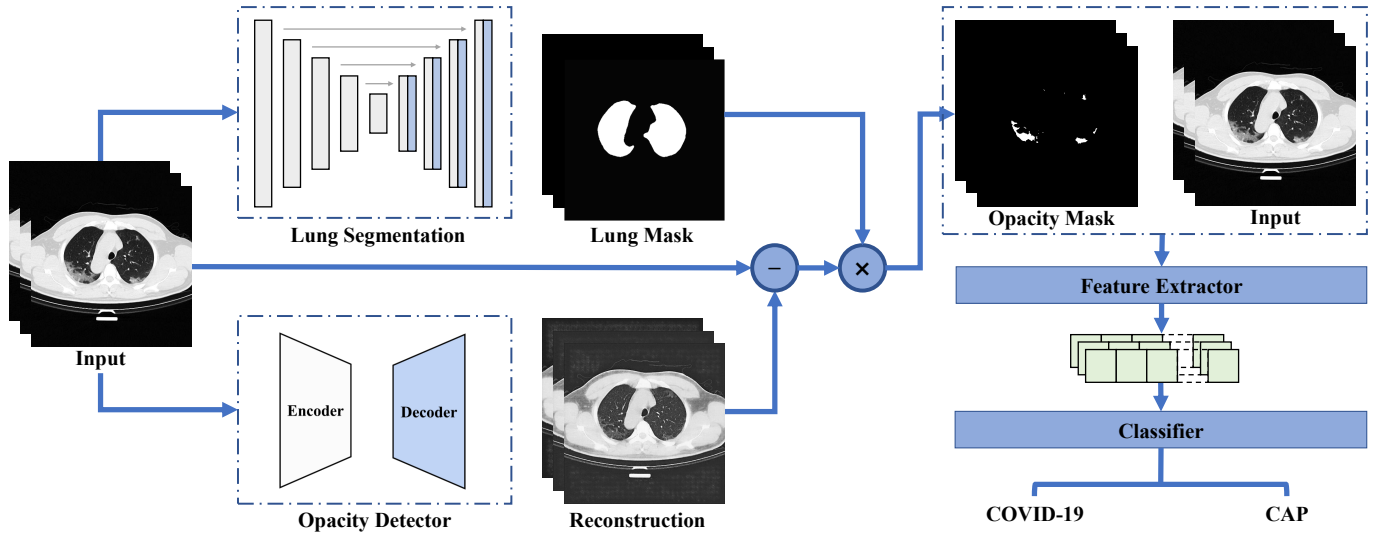
Fig. 1. An overview of the proposed method. The input CT slices are fed into lung segmentation model and opacity detector respectively. The differences between the reconstructed images obtained from opacity detection model and original images are computed and multiplied by segmentation results. After thresholding, binary masks generated from difference maps incorporate with original images are utilized for feature extraction and classification to get the final results.

TABLE I
DATASETS USED TO TRAIN AND EVALUTE THE PERFORMANCE OF LUNG SEGMENTATION MODEL.

Name	Description	Volumes	Split
LCTSC	Chest CT scans from cancer patients of three different institutions	60	Train
VESSEL12	Chest CT scans contain abnormalities such as emphysema and nodules	20	Train
StructSeg	Chest CT scans from cancer patients	50	Train
DLDsOsaka	Scans contain seven categories of pulmonary textures	217	Train&Test
COVID-19-CT-Seg	Chest CT scans diagnosed as COVID-19	20	Test
COVID-19-ZJU	COVID-19 CT scans collected by Zhejiang University	16	Test

Dataset. Depending on the severity of COVID-19 and CAP, the typical pulmonary texture can be categorized into ground glass opacities (GGO), crazy-paving and consolidation (CON). To this end, we collect data from different datasets to build a generalized dataset that covers most of the abnormalities in lungs, as shown in the Table I. The lung CT segmentation challenge 2017 (LCTSC) [26] contains CT images from 60 cancer patients of three different institutions. The vessel segmentation in the lung 2012 (VESSEL12) [27] provides a total of 20 segmented lungs with abnormalities such as emphysema, nodules and pulmonary embolisms. The automatic structure segmentation for radiotherapy planning challenge (Struct-Seg) [28] published 50 cases from cancer patients. The diffuse lung diseases collected from Osaka University (DLDsOsaka) contains seven categories of pulmonary textures including consolidation (CON), honeycombing (HCM), nodular opacity (NOD), emphysema (EMP), multi-focal ground glass opacity (MGGO), reticular ground glass opacity (RGGO) and normal pulmonary tissues (NOR). To evaluate the generalization of the trained model and the diversity of the training data, we build a test dataset that consists of two COVID-19 datasets and a part of DLDsOsaka (10% cases are randomly sampled). The COVID-19 CT segmentation (COVID-19-CT-Seg) provides

CT scans from 20 patients infected with COVID-19. The COVID-19-ZJU dataset is collected by Zhejiang University contains 16 CT volumes diagnosed as COVID-19.

Implementation details. We perform segmentation on 2D slice. During training and inference, the CT image intensity values are clipped to the window $[-600, 1500]$ and normalized to $[0, 1]$. All images are rescaled to a resolution of 512×512 pixels. Several image augmentations are applied during training, such as, random rotation, Gauss noise, random contrast, blur and sharpen. Among the training data, about 90% are used for training, while the rest 10% is used for validation. The learning rate is 1e-4 and batch size is 16. Adam [29] is used for optimization. The proposed network is implemented by PyTorch [30] framework. All experiments are performed on a TITAN RTX GPU.

Evaluation metrics. In this paper, the performance of the segmentation network is conducted by the Dice similarity coefficient (DSC). The metric is defined as follows:

$$DSC(A, B) = \frac{2\,|A \cap B|}{|A| + |B|} \qquad (1)$$

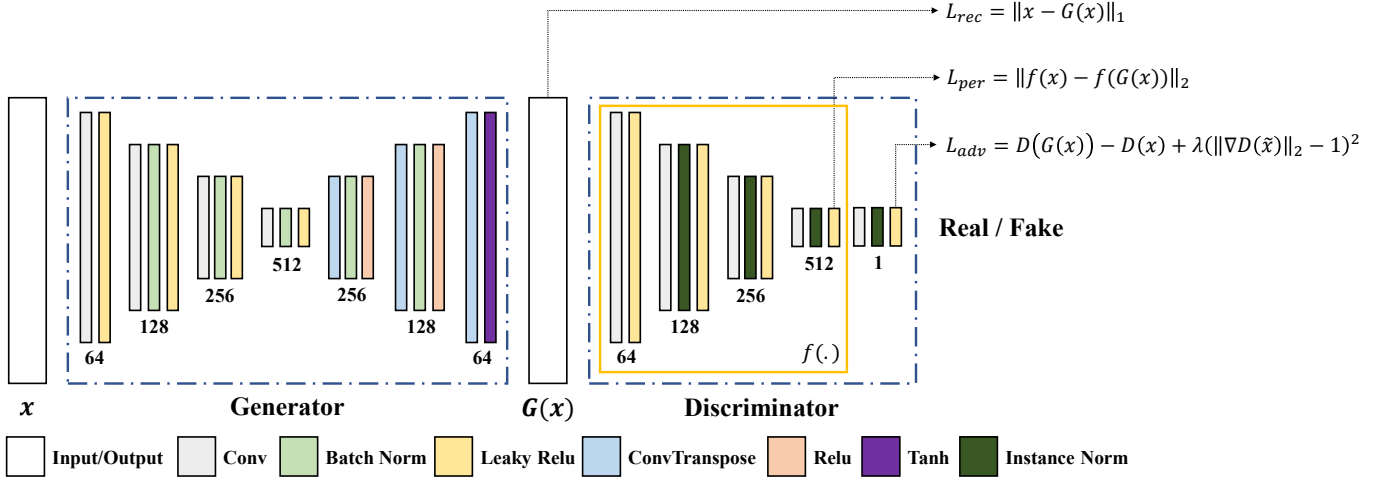where A is the segmented region, B denotes the corresponding ground-truth.

Fig. 2. The architecture of the proposed opacity detection model which contains an auto-encoder and an encoder, employed within two sub-networks. First sub-network behaves as the generator part of the model. The second sub-network is the discriminator network whose objective is to identify the input x and the output output $G(x)$ as real or reconstructed.

B. Opacity detection

Models. We build a GAN-based auto-encoder to identify opacites. The network consists of two sub-networks, a generator G and discriminator D (see Figure 2). First sub-network is an auto-encoder network aims at mapping the CT images with normal lung tissues to latent space and remapping back to its reconstructions. To fully reconstruct the healthy CT images and model the distribution of the normal data, the second sub-network is introduced behaving as the discriminator part of the opacity detection model. The discriminator is trained directly on real and reconstructed images and is responsible for classifying images as real or fake (reconstructed). The two sub-networks compete in a two-player game where the generator tries to fool the discriminator while the discriminator learns to distinguish between real and reconstructed data and simultaneous improvements are made to both sub-networks.

Loss function. The objective function consists of three loss functions, reconstruction loss L_{rec}, perceptual loss L_{per} and adversarial loss L_{adv}. The formal definition of the objective function is as follows: Given an input x drawn from normal data distribution $p_{\mathbf{X}}$, we penalize G by minimizing the pixel-wise l_1-distance between the original x and the reconstructed images $G(x)$ to encourage the generator to learn contextual information about the input data which is defined by:

$$L_{rec} = \mathbb{E}_{x \sim p_{\mathbf{X}}} \|x - G(x)\|_1 \tag{2}$$

Inspired by [14] [31] that GAN training tends to be stable by reducing the intermediate outputs from discriminator D, we propose a new perceptual loss to reuse the feature maps computed by discriminator. Perceptual loss [32] measures the distance of features obtained from a pre-trained network which is widely applied in image translation task. Here, we use the features output from an intermediate layer of the discriminator defined as f. We penalize G to match the feature

representation between the real and reconstructed images. Hence, the perceptual loss L_{per} is defined as:

$$L_{per} = \mathbb{E}_{x \sim p_{\mathbf{X}}} \|f(x) - f(G(x))\|_2 \tag{3}$$

Gulrajani *et al.* [33] proposed improved Wasserstein distance with gradient penalty to enforce the Lipschitz constraint for the stable training of GAN. Hence, we refer to the design of WGAN-GP's loss function to constrain discriminator which is defined as follows:

$$L_{adv} = \mathbb{E}_{x \sim p_{\mathbf{X}}} D(G(x)) - \mathbb{E}_{x \sim p_{\mathbf{X}}} D(x) + \tag{4}$$
$$\lambda (\mathbb{E}_{\tilde{x} \sim p_{\tilde{\mathbf{X}}}} \|\nabla D(\tilde{x})\|_2 - 1)^2$$

where lambda is the weighting parameters, $p_{\tilde{\mathbf{X}}}$ is the generator distribution and $\tilde{x}$ sampled from $G(x)$ and x with t uniformly sampled between $[0, 1]$:

$$\tilde{x} = tG(x) + (1 - t)x \tag{5}$$

Overall, the objective function for opacity detection becomes the following:

$$L = \lambda_{rec} L_{rec} + \lambda_{per} L_{per} + \lambda_{adv} L_{adv} \tag{6}$$

where λ_{rec}, λ_{per} and λ_{adv} are the weights to balance the impact to the overall objective function.

Dataset. We collect healthy CT scans from 30 cases in DLDsOsaka dataset for training. CT images of a total of 200 participants are collected for testing. In test set, there are 100 confirmed COVID-19 cases and the other 100 cases are CAP patients. Five hospitals are involved, including Zhejiang Hospital, Hangzhou Second People's Hospital, Jingmen First People's Hospital, Taizhou Hospital and Sir Run Run Shaw Affiliated Hospital of Zhejiang University School of Medicine.

Implementation details. To better reconstruct the input data, we train the opacity detection model based on 2D image patches extracted from CT volumes. During inference, full size images are fed into the model to get the reconstructed
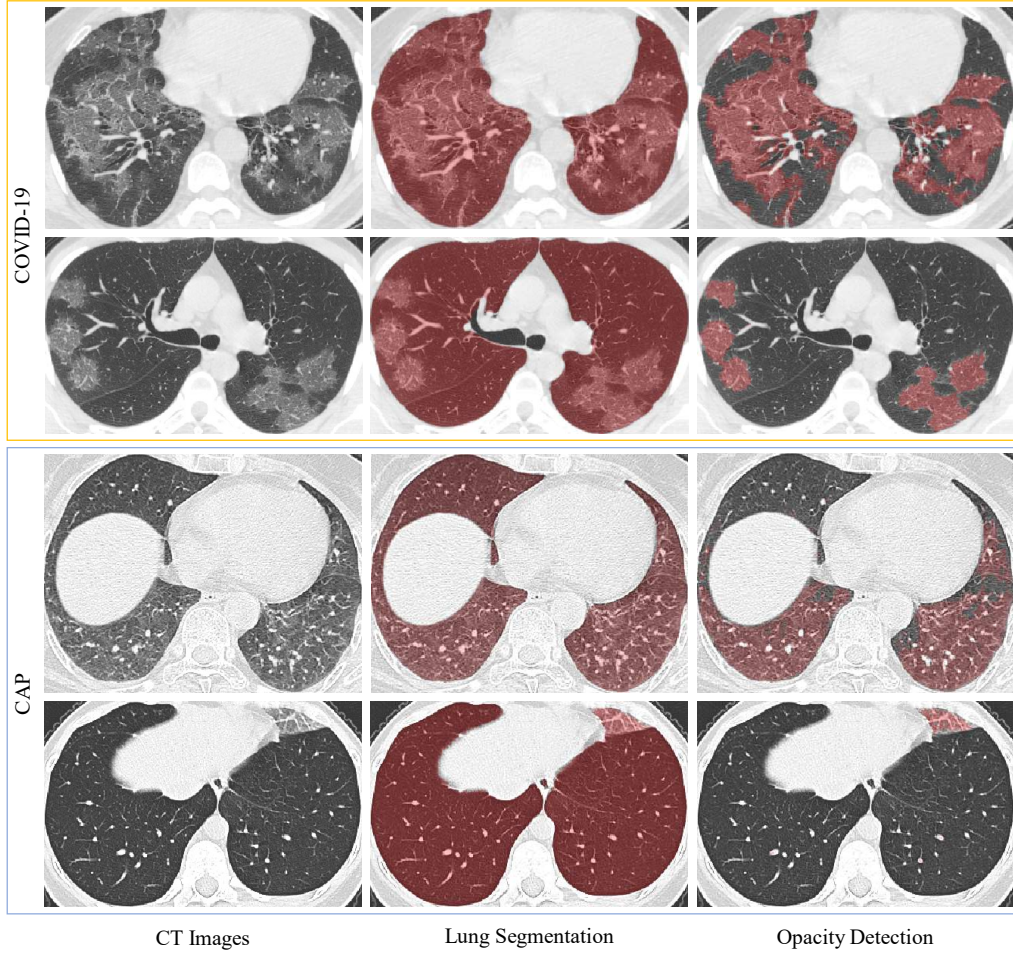
Fig. 3. Visualization of segmentation and opacity detection results on COVID-19 and CAP cases.

abnormal images. By carefully constructing fully convolutional networks, the model can take input of arbitrary size and produce correspondingly-sized output. All CT images are resized to 512×512 resolution and the intensity values are clipped to lung window $[-600, 1500]$ and mapped to $[0, 1]$. Image patches are extracted according to the following procedure. Raster-scanning with 32 pixels stride is used to extract image patches with the size of $64 \times 64 \times 1$. Patches are further selected if the centers of image patches are inside the lung regions produced by the segmentation model. Finally, a total of 444755 $64 \times 64 \times 1$ image patches are utilized to train the model. To reduce unnecessary noises which may impact the quality of reconstructions, median filter is used before extracting patches for training and testing data.

Inference. During test stage, the difference map is computed between the reconstructed output of generator $G(x)$ and abnormal input x and then normalized to $[0, 1]$ to get a probability map. Each pixel in the probability map represents an opacity score. After thresholding and multiplied by segmentation map, a binary mask of opacity in lung region can be converted from the probability map as the final output of opacity detection model.

C. Feature Extractor and Classifier

Feature Extractor. We apply radiomics [34] feature extraction on opacity regions determined by opacity detection model. Same features are also extracted from lung regions for comparison. We extract features from three different transformed images including original image, image transformed by Laplacian of Gaussian (LoG) filter and image transformed by wavelet. Seven classes of features are selected for each transformed image: first order statistics, shape-based features, gray level co-occurrence matrix (GLCM), gray level run length matrix (GLRLM), gray level size zone matrix (GLSZM), gray level dependence matrix (GLDM) and neighboring gray tone difference matrix (NGTDM). Finally, we obtain a total of 1023-dimensional features. After that, least absolute shrinkage and selection operator (LASSO) [15] is employed to filter out redundant and unnecessary features and the remaining features are used for classification.

Classifier. In our experiments, we compare the features extracted from opacity regions and lung regions with the following machine learning methods. Support vector machine [35] with a linear kernel (Linear SVM) or a radial basis function kernel (RBF SVM), random forest [36], adaptive boosting

(AdaBoost) [37] and XGBoost [38]. For all classifiers, we employ a 5-fold cross-validation strategy to evaluate the performance.

Evaluation metrics. Classification performance is evaluated by four evaluation metrics, including accuracy, precision, recall, f1-score and the area under the receiver operating characteristic curve (AUC). Given true positive (TP), true negative (TN), false positive (FP) and false negative (FN), the accuracy, precision, recall and f1-score are calculated as follows:

$$Accuracy = \frac{TP + TN}{TP + TN + FP + FN} \tag{7}$$

$$Precision = \frac{TP}{TP + FP} \tag{8}$$

$$Recall = \frac{TP}{TP + FN} \tag{9}$$

$$F1 - score = 2 \times \frac{Recall \times Precision}{Recall + Precision} \tag{10}$$

IV. RESULTS

In this section, we conduct experiments including quantitative results and qualitative results to demonstrate the effectiveness of our proposed method.

A. Lung Segmentation

We show the quantitative results obtained by segmentation model in Table II. The best performance is marked by bold letters. The results show that models trained on our training sets generalize well to test sets with different backbones. To achieve a better trade-off between accuracy and speed, we finally choose MobileNetV2 as the backbone of the segmentation model. Figure 4 shows qualitative results for cases from test sets. Our segmentation model yields masks that are close to the ground truth.
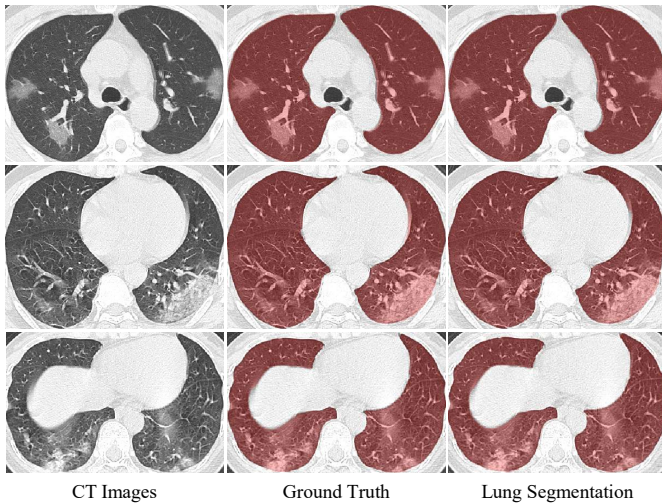

CT Images   Ground Truth   Lung Segmentation

Fig. 4. Visualization of segmentation results.

TABLE II
QUANTITATIVE RESULTS OF LUNG SEGMENTATION.

Backbone	DLDsOsaka	COVID-19-CT-Seg	COVID-19-ZJU
MobileNetV2	0.98411	0.98168	**0.99229**
VGG19	**0.98504**	**0.98174**	0.99136
ResNet50	0.98473	0.98159	0.99116

B. Opacity Detection

Figure 3 illustrates the lung regions obtained from segmentation model and opacity regions detected by opacity detection model. As can be observed, opacities in lung regions from patients diagnosed with COVID-19 or CAP can be segmented correctly. Without the need for training in a supervised manner, the proposed opacity detection model has ability to produce accurate opacity masks by training only on CT images with normal lung tissues. The obtained results demonstrate the effectiveness of the opacity detection model.

C. Classification

To demonstrate that extracting features from opacity regions rather than the entire lung regions contributes to improving the performance of classification, we conduct experiments on two different types of features for classifier, including lung-specific features and opacity-specific features. Table III exhibits the quantitative results (accuracy,precision, recall, f1-score and AUC) achieved by different machine learning methods. Specifically, the performance of using opacity-specific features is higher than lung-specific on most of classification models. In terms of accuracy, RBF SVM with opacity-specific features achieves the best result, up to 95.5%. Therefore, the promising performance validate that the proposed method can diagnose COVID-19 from CAP accurately.

D. Limitations

Although the proposed opacity detection model for diagnosis of COVID-19 has achieved promising results. There are still cases that opacity detection can not detect the opacity regions correctly. Figure 5 gives some examples of the failure cases. We can observe that opacity detection failed when encountering patients with severe COVID-19 pneumonia. The reconstructed images shown in Figure 5 indicates that the reason for failing to find opacity regions is that the textures of opacities are too close to the textures of regions outside lung. A possible solution could be to modify the contrast between the regions inside and outside lung before fed into opacity detection model.

V. CONCLUSION

In this paper, we propose an opacity detection model for diagnosis of COVID-19. By applying opacity detection, the opacity regions can be segmented in an unsupervised manner which is a key to overcome the bottleneck of insufficient labeled data. We conduct experiments for investigating the effectiveness of opacity-specific features for classification. The

| Methods	Feature Extraction		Evaluation				
	Lung	Opacity	Accuracy	Precision	Recall	F1-score	AUC
Linear SVM	✓		0.9350	0.9674	**0.9000**	0.9302	0.9565
		✓	**0.9400**	**0.9905**	0.8900	**0.9338**	**0.9585**
RBF SVM	✓		0.9350	0.9674	0.9000	0.9302	0.9565
		✓	**0.9550**	**1.0000**	**0.9100**	**0.9510**	**0.9590**
Random Forest	✓		0.9400	0.9889	0.8900	0.9342	0.9640
		✓	**0.9450**	**0.9895**	**0.9000**	**0.9402**	**0.9720**
AdaBoost	✓		0.9200	0.9285	**0.9100**	0.9178	0.9620
		✓	**0.9400**	**0.9714**	**0.9100**	**0.9372**	**0.9640**
XGBoost	✓		0.9200	0.9443	0.8900	0.9155	0.9560
		✓	**0.9450**	**0.9800**	**0.9100**	**0.9416**	**0.9600**
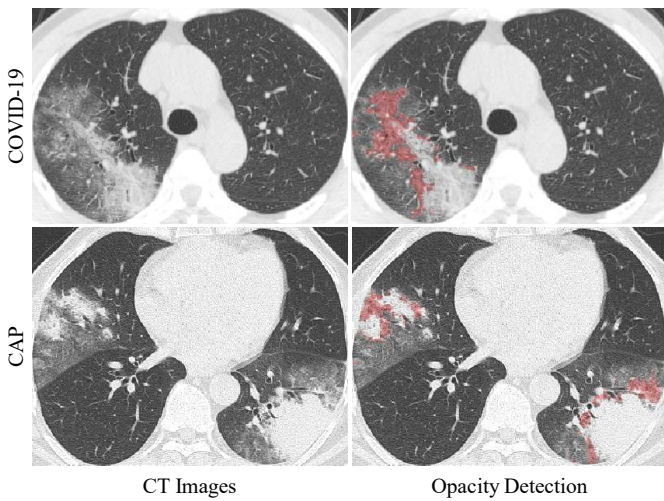
Fig. 5. Relatively low detection performance of opacity detection on some cases from COVID-19 and CAP.

results on the collected COVID-19 dataset with 100 COVID-19 cases and 100 CAP cases demonstrated that diagnosis performance is promoted with features extracted from opacity regions. In the future, we plan to improve the performance of opacity detection model and integrate more data into our framework for accuracy promotion.

ACKNOWLEDGEMENT

REFERENCES

[1] Z. Y. Zu, M. D. Jiang, P. P. Xu *et al.*, "Coronavirus disease 2019 (covid-19): a perspective from china," *Radiology*, p. 200490, 2020.

[2] C. Sohrabi, Z. Alsafi, N. O'Neill *et al.*, "World health organization declares global emergency: A review of the 2019 novel coronavirus (covid-19)," *International Journal of Surgery*, vol. 76, 2020.

[3] Y. Li and L. Xia, "Coronavirus disease 2019 (covid-19): role of chest ct in diagnosis and management," *American Journal of Roentgenology*, vol. 214, no. 6, pp. 1280–1286, 2020.

[4] Y. Fang, H. Zhang, J. Xie *et al.*, "Sensitivity of chest ct for covid-19: comparison to rt-pcr," *Radiology*, p. 200432, 2020.

[5] T. Ai, Z. Yang, H. Hou *et al.*, "Correlation of chest ct and rt-pcr testing in coronavirus disease 2019 (covid-19) in china: a report of 1014 cases," *Radiology*, p. 200642, 2020.

[6] C. Zheng, X. Deng, Q. Fu *et al.*, "Deep learning-based detection for covid-19 from chest ct using weak label," *medRxiv*, 2020.

[7] S. Wang, B. Kang, J. Ma *et al.*, "A deep learning algorithm using ct images to screen for corona virus disease (covid-19)," *medRxiv*, 2020.

[8] U. Ozkaya, S. Ozturk, and M. Barstugan, "Coronavirus (covid-19) classification using deep features fusion and ranking technique," *arXiv preprint arXiv:2004.03698*, 2020.

[9] S. H. Kassani, P. H. Kassasni, M. J. Wesolowski *et al.*, "Automatic detection of coronavirus disease (covid-19) in x-ray and ct images: A machine learning-based approach," *arXiv preprint arXiv:2004.10641*, 2020.

[10] M. Farooq and A. Hafeez, "Covid-resnet: A deep learning framework for screening of covid19 from radiographs," *arXiv preprint arXiv:2003.14395*, 2020.

[11] L. Sun, Z. Mo, F. Yan *et al.*, "Adaptive feature selection guided deep forest for covid-19 classification with chest ct," *arXiv preprint arXiv:2005.03264*, 2020.

[12] X. Ouyang, J. Huo, L. Xia *et al.*, "Dual-sampling attention network for diagnosis of covid-19 from community acquired pneumonia," *IEEE Transactions on Medical Imaging*, 2020.

[13] F. Shi, L. Xia, F. Shan *et al.*, "Large-scale screening of covid-19 from community acquired pneumonia using infection size-aware classification," *arXiv preprint arXiv:2003.09860*, 2020.

[14] S. Akcay, A. Atapour-Abarghouei, and T. P. Breckon, "Ganomaly: Semi-supervised anomaly detection via adversarial training," in *Asian conference on computer vision*. Springer, 2018, pp. 622–637.

[15] R. Tibshirani, "Regression shrinkage and selection via the lasso," *Journal of the Royal Statistical Society: Series B (Methodological)*, vol. 58, no. 1, pp. 267–288, 1996.

[16] N. Pawlowski, M. C. Lee, M. Rajchl *et al.*, "Unsupervised lesion detection in brain ct using bayesian convolutional autoencoders," in *Medical Imaging with Deep Learning*, 2018.

[17] T. Schlegl, P. Seeböck, S. M. Waldstein *et al.*, "Unsupervised anomaly detection with generative adversarial networks to guide marker discovery," in *International conference on information processing in medical imaging*. Springer, 2017, pp. 146–157.

[18] X. Chen and E. Konukoglu, "Unsupervised detection of lesions in brain mri using constrained adversarial auto-encoders," *arXiv preprint arXiv:1806.04972*, 2018.

[19] X. Chen, S. You, K. C. Tezcan *et al.*, "Unsupervised lesion detection via image restoration with a normative prior," *Medical Image Analysis*, p. 101713, 2020.

[20] C. Baur, B. Wiestler, S. Albarqouni *et al.*, "Deep autoencoding models for unsupervised anomaly segmentation in brain mr images," in *International MICCAI Brainlesion Workshop*. Springer, 2018, pp. 161–169.

[21] D. Sato, S. Hanaoka, Y. Nomura *et al.*, "A primitive study on unsupervised anomaly detection with an autoencoder in emergency head ct volumes," in *Medical Imaging 2018: Computer-Aided Diagnosis*, vol. 10575. International Society for Optics and Photonics, 2018, p. 105751P.

[22] O. Ronneberger, P. Fischer, and T. Brox, "U-net: Convolutional networks for biomedical image segmentation," in *International Conference on Medical image computing and computer-assisted intervention*. Springer, 2015, pp. 234–241.

[23] M. Sandler, A. Howard, M. Zhu *et al.*, "Mobilenetv2: Inverted residuals and linear bottlenecks," in *Proceedings of the IEEE conference on computer vision and pattern recognition*, 2018, pp. 4510–4520.

[24] K. Simonyan and A. Zisserman, "Very deep convolutional networks for large-scale image recognition," *arXiv preprint arXiv:1409.1556*, 2014.

[25] K. He, X. Zhang, S. Ren *et al.*, "Deep residual learning for image recognition," in *Proceedings of the IEEE conference on computer vision and pattern recognition*, 2016, pp. 770–778.

[26] J. Yang, H. Veeraraghavan, S. G. Armato III *et al.*, "Autosegmentation for thoracic radiation treatment planning: A grand challenge at aapm 2017," *Medical physics*, vol. 45, no. 10, pp. 4568–4581, 2018.

[27] R. D. Rudyanto, S. Kerkstra, E. M. Van Rikxoort *et al.*, "Comparing algorithms for automated vessel segmentation in computed tomography scans of the lung: the vessel12 study," *Medical image analysis*, vol. 18, no. 7, pp. 1217–1232, 2014.

[28] "Automatic structure segmentation," 2019. [Online]. Available: http://structseg-challenge.org/#/

[29] D. P. Kingma and J. Ba, "Adam: A method for stochastic optimization," *arXiv preprint arXiv:1412.6980*, 2014.

[30] A. Paszke, S. Gross, S. Chintala *et al.*, "Automatic differentiation in pytorch," in *Advances in neural information processing systems*, 2017.

[31] T. Salimans, I. Goodfellow, W. Zaremba *et al.*, "Improved techniques for training gans," in *Advances in neural information processing systems*, 2016, pp. 2234–2242.

[32] J. Johnson, A. Alahi, and L. Fei-Fei, "Perceptual losses for real-time style transfer and super-resolution," in *European conference on computer vision*. Springer, 2016, pp. 694–711.

[33] I. Gulrajani, F. Ahmed, M. Arjovsky *et al.*, "Improved training of wasserstein gans," in *Advances in neural information processing systems*, 2017, pp. 5767–5777.

[34] J. J. Van Griethuysen, A. Fedorov, C. Parmar *et al.*, "Computational radiomics system to decode the radiographic phenotype," *Cancer research*, vol. 77, no. 21, pp. e104–e107, 2017.

[35] C. Cortes and V. Vapnik, "Support-vector networks," *Machine learning*, vol. 20, no. 3, pp. 273–297, 1995.

[36] L. Breiman, "Random forests," *Machine learning*, vol. 45, no. 1, pp. 5–32, 2001.

[37] Y. Freung and R. Shapire, "A decision-theoretic generalization of online learning and an application to boosting," *J Comput Syst Sci*, vol. 55, pp. 119–139, 1997.

[38] T. Chen and C. Guestrin, "Xgboost: A scalable tree boosting system," in *Proceedings of the 22nd acm sigkdd international conference on knowledge discovery and data mining*, 2016, pp. 785–794.